Supplementary Information

HDAC6 Controls Fat-induced Lipid Storage by Regulating CIDEC Acetylation and Stability

Hui Qian[1]*, Yuanying Chen[1]*, Zongqian Nian[1]*, Lu Su[1], Haoyong Yu[2], Feng-Jung Chen[1], Xiuqin Zhang[3], Wenyi Xu[1], Linkang Zhou[1], Jiaming Liu[1], Jinhai Yu[1], Luxin Yu[1], Yan Gao[4], Hongchao Zhang[5], Haihong Zhang[5], Shimin Zhao[7], Li Yu[8], Rui-Ping Xiao[9], Yuqian Bao[2], Shaocong Hou[10], Pingping Li[10], Jia Da Li[11], Haiteng Deng[4], Weiping Jia[2] and Peng Li[1#]

[1]MOE key laboratory of Bioinformatics and Tsinghua-Peking Center for Life Sciences, School of Life Sciences, Tsinghua University, Beijing, 100084, China; [2]Shanghai Key Laboratory of Diabetes Mellitus, Department of Endocrinology and Metabolism, Shanghai JiaoTong University Affiliated Sixth People's Hospital, Shanghai Diabetes Institute, Shanghai Clinical Center for Diabetes, and Shanghai Key Clinical Center for Metabolic Disease, Shanghai 200233, China; [3]Institute of Molecular Medicine, Beijing Key Laboratory of Cardiometabolic Molecular Medicine, Peking University, Beijing, 100871, China; [4]Proteomics Facility, School of Life Sciences, Tsinghua University, Beijing 100084, China; [5]Department of Heart Center, Air Force General Hospital, PLA, Beijing 100142, China; [6]Department of General Surgery, Air Force General Hospital, PLA, Beijing 100142, China; [7]State Key Laboratory of Genetic Engineering, School of Life Sciences, Institutes of Biomedical Sciences, Fudan University, Shanghai 200032, China; [8]State Key Laboratory of Biomembrane and Membrane Biotechnology, Tsinghua University-Peking University Joint Center for Life Sciences, School of Life Sciences, Tsinghua University, Beijing 100084, China; [9]Institute of Molecular Medicine, State Key Laboratory of Biomembrane and Membrane Biotechnology, Peking-Tsinghua Center for Life Sciences, Beijing Key Laboratory of Cardiometabolic Molecular Medicine, Peking University, Beijing, 100871, China; [10]State Key Laboratory of Bioactive Substance and Function of Natural Medicines, Institute of Materia Medica, Chinese Academy of Medical Sciences and Peking Union Medical College, Diabetes Research Center of Chinese Academy of Medical Sciences, Beijing, 100050, China; [11]The State Key Laboratory of Medical Genetics and School of Life Sciences, Central South University, 110 Xiangya Road, Changsha, Hunan, 410078, China.

* These authors contributed equally to this work.
#Address correspondence to: Dr. Peng Li, School of Life Sciences, Tsinghua University, HaiDian District, Beijing 100084, China. Tel: 86-10-62797121; E-mail: li-peng@mail.tsinghua.edu.cn

List:

Supplemental Figures and legends
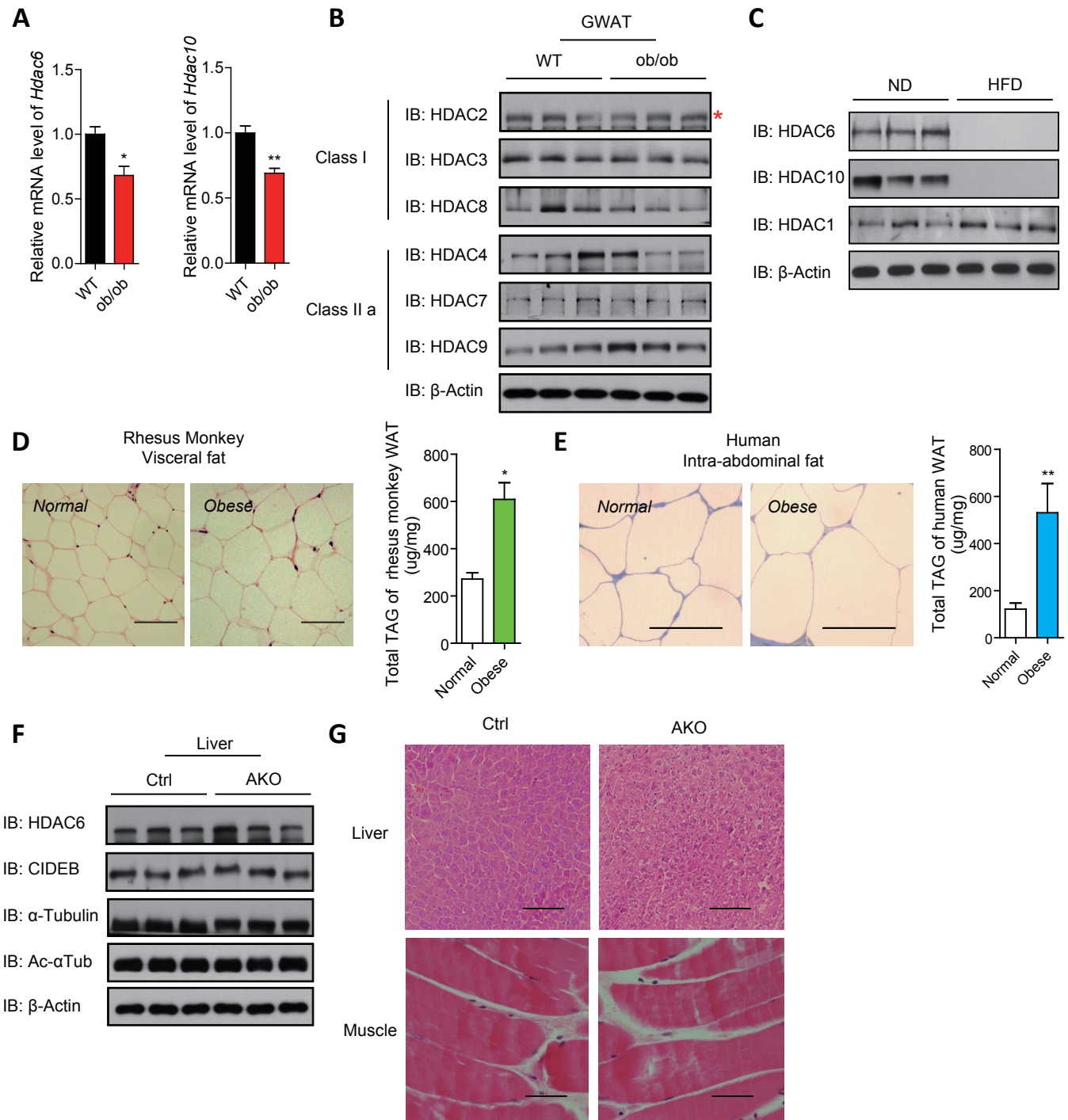
Supplemental Experimental Procedures

Statistical analyses for comparison of oxygen consumption.
Supplemental Methods.

Data sheet S1

Summary of the acetylated-protein in *Hdac6* adipose tissue konckout mice related with lipid metabolism
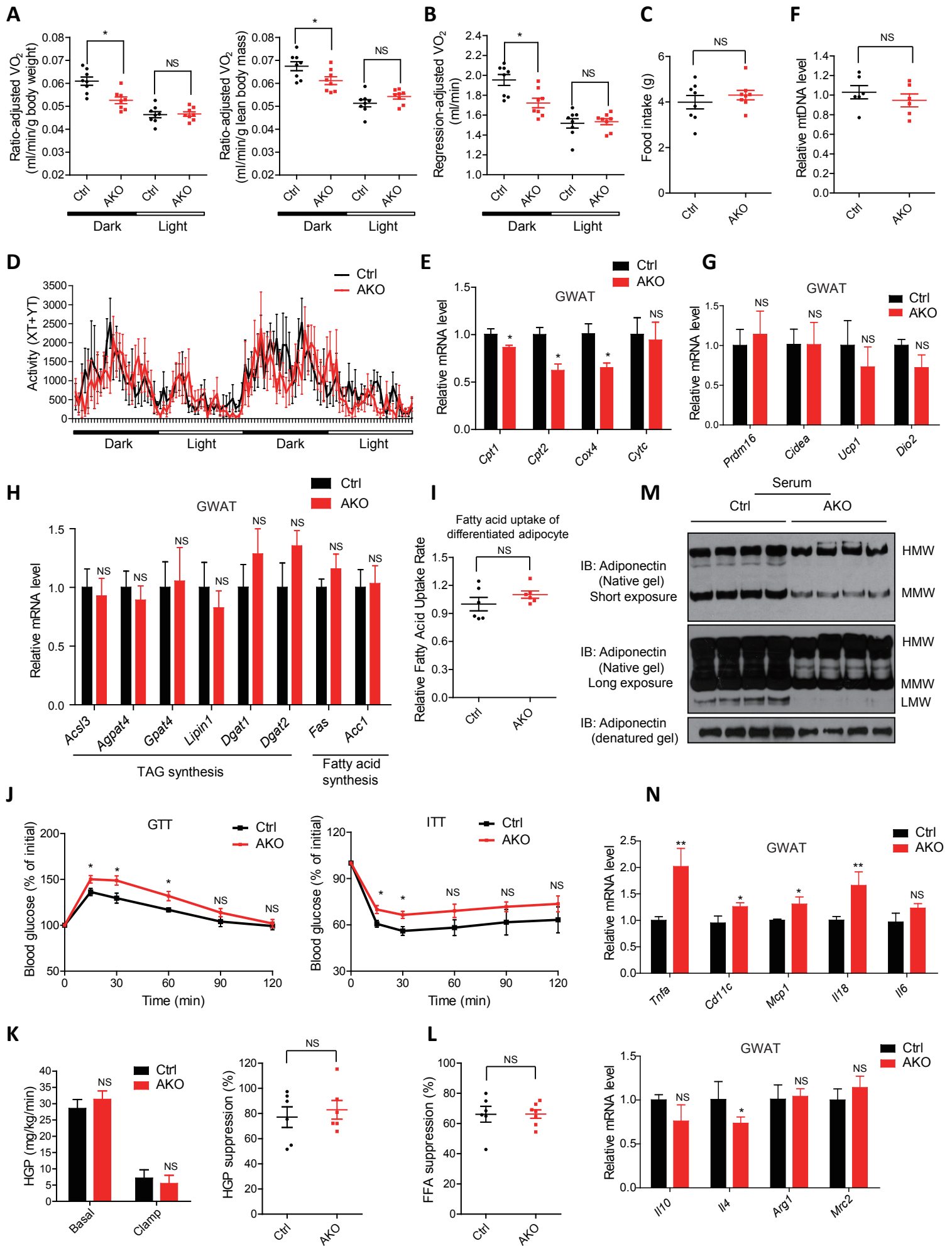
Supplemental Figure 1

A

B

C

D Rhesus Monkey Visceral fat

E Human Intra-abdominal fat

F

G

Supplemental Figure 1. Related to Figure 1. Negative correlation between HDAC6 and obesity.

(**A**) Relative mRNA levels of *Hdac6* and *Hdac10* in the GWAT of *ob/ob* mice (n=4 mice per group).

(**B**) Levels of Class I and Class IIa HDACs proteins in the gonadal white fat (GWAT) of leptin deficient (*ob/ob*) mice. GWAT was dissected from 4-month old wild-type and leptin deficient (*ob/ob*) mice (n=3 mice per group).

(**C**) Reduced HDAC6 and HDAC10 levels in the GWAT of high fat diet (HFD)-fed mice (n=3 mice per group).

(**D**) Morphology (by H&E staining) and total TAG levels of visceral fat of normal and obese rhesus monkeys (n=3 rhesus monkeys per group). Scale bars represent 50 μm.

(**E**) Electron microscopic image of semi-thin section and total TAG content of intra-abdominal (omental) adipose tissue from normal and obese individual (n=3 human samples per group). Scale bars represent 50 μm.

(**F**) HDAC6 protein expression in the liver of the Ctrl and the AKO mice. Levels of α-Tubulin acetylation was used as a control (n=3 mice per group).

(**G**) The morphology of the liver and muscle in the Ctrl and the AKO mice (n=3 mice per group). Scale bars represent 50 μm.

Data represent the mean ± SEM. Statistical difference was indicated as *$P < 0.05$, **$P < 0.01$, ***$P < 0.001$, by two-tailed Student's *t* test.
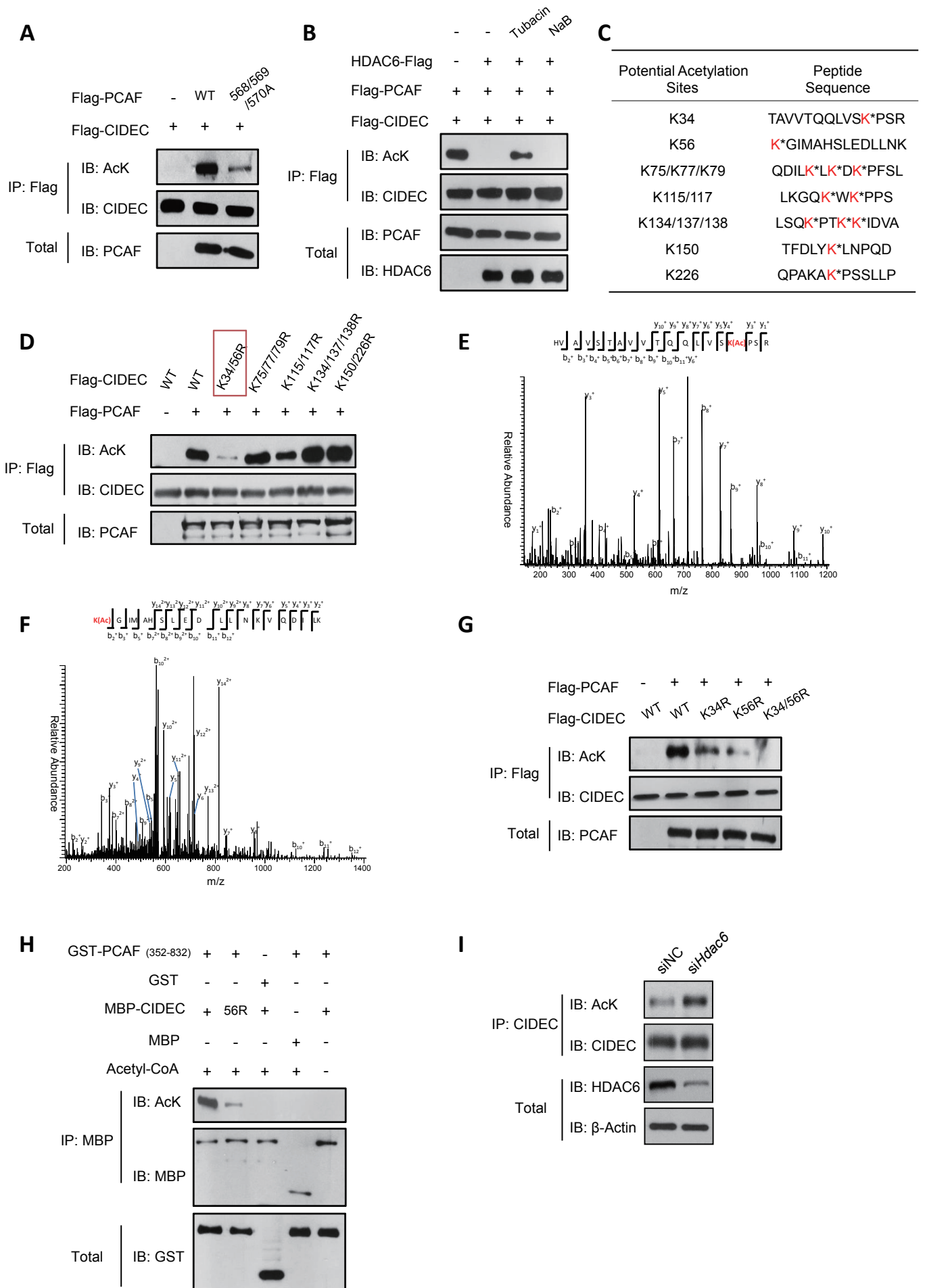
Supplemental Figure 2

Supplemental Figure 2. Related to Figure 2. Animals with adipose tissue specific knockout of *Hdac6* have decreased metabolic activity and lower insulin sensitivity.

(**A**) Oxygen consumption of control (Ctrl) and AKO mice using the body weight or lean body mass ratio-based method, respectively (n=8 mice per group).

(**B**) Regression adjusted oxygen consumption of control (Ctrl) and AKO mice (n=8 mice per group).

(**C**) Food intake of the control and AKO mice (n=8 mice per group).

(**D**) Physical activity of control and AKO mice (n=8 mice per group).

(**E**) Expression levels of genes in mitochondrial oxidative pathway in the adipose tissue of the Ctrl and the AKO mice (n=6 mice per group).

(**F**) Relative mitochondrial DNA (mtDNA) copy number analysis using real-time PCR (n=6 mice per group).

(**G**) Expression levels of adipose beiging maker genes (n=6 mice per group).

(**H**) Expression levels of genes in TAG synthesis pathway and fatty acid biosynthesis pathway (n=6 mice per group).

(**I**) Fatty acid uptake in the adipocytes of the Ctrl and the AKO mice (n=6 mice per group).

(**J**) Glucose tolerance test (GTT) and insulin tolerance test (ITT) (n=8 mice per group).

(**K**) Levels of hepatic glucose production (HGP) and HGP suppression for the Ctrl and the AKO mice (n=6 mice per group).

(**L**) Levels of free fatty acid (FFA) suppression of the Ctrl and the AKO mice (n=6 mice per group).

(**M**) Native gel to show serum levels of high molecular weight (HMW) and medium molecular weight (MMW) adiponectin (n=4 mice per group).

(**N**) Expression levels of genes in inflammatory pathway (n=6 mice per group).

Data represent the mean $\pm$ SEM. Statistical difference was indicated as *$P < 0.05$, **$P < 0.01$, ***$P < 0.001$, by two-tailed Student's *t* test.
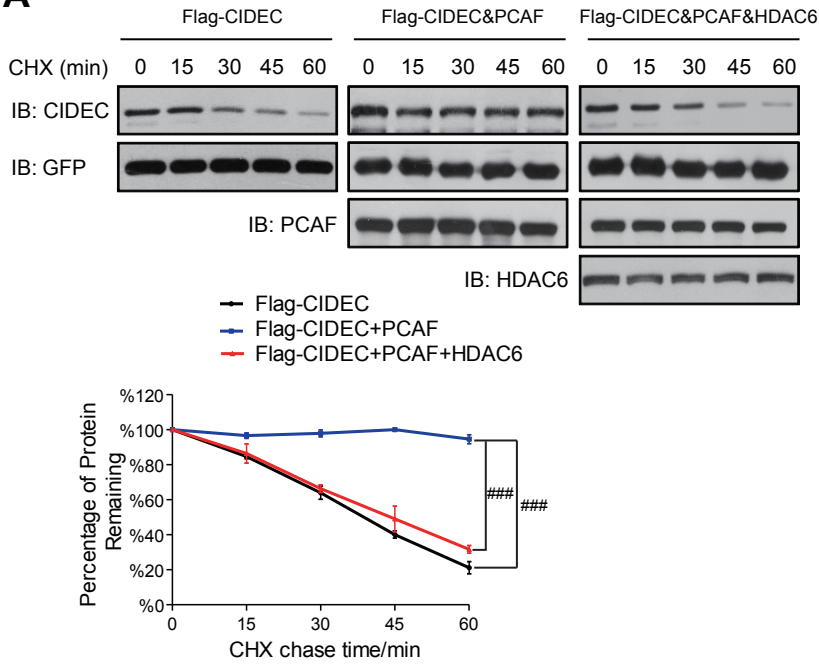
Supplemental Figure 3

A

Flag-PCAF: −, WT, 568/569/570A
Flag-CIDEC: +, +, +

IP: Flag
IB: AcK
IB: CIDEC

Total
IB: PCAF

B

HDAC6-Flag: −, +, +, +
Flag-PCAF: +, +, +, +
Flag-CIDEC: +, +, +, +
(−, −, Tubacin, NaB)

IP: Flag
IB: AcK
IB: CIDEC

Total
IB: PCAF
IB: HDAC6

C

Potential Acetylation Sites	Peptide Sequence
K34	TAVVTQQLVSK*PSR
K56	K*GIMAHSLEDLLNK
K75/K77/K79	QDILK*LK*DK*PFSL
K115/117	LKGQK*WK*PPS
K134/137/138	LSQK*PTK*K*IDVA
K150	TFDLYK*LNPQD
K226	QPAKAK*PSSLLP

D

Flag-CIDEC: WT, WT, K34/56R, K75/77/79R, K115/117R, K134/137/138R, K150/226R
Flag-PCAF: −, +, +, +, +, +, +

IP: Flag
IB: AcK
IB: CIDEC

Total
IB: PCAF

E

HV A V S T A V V T Q Q L V S K(Ac) P S R

Relative Abundance vs m/z

F

K(Ac) G IM AH S L E D L L F N K V Q D F L K

Relative Abundance vs m/z

G

Flag-PCAF: −, +, +, +, +
Flag-CIDEC: WT, WT, K34R, K56R, K34/56R

IP: Flag
IB: AcK
IB: CIDEC

Total
IB: PCAF

H

GST-PCAF (352-832): +, +, −, +, +
GST: −, −, +, −, −
MBP-CIDEC: +, 56R, +, −, +
MBP: −, −, −, +, −
Acetyl-CoA: +, +, +, +, −

IP: MBP
IB: AcK
IB: MBP

Total
IB: GST

I

siNC, siHdac6

IP: CIDEC
IB: AcK
IB: CIDEC

Total
IB: HDAC6
IB: β-Actin

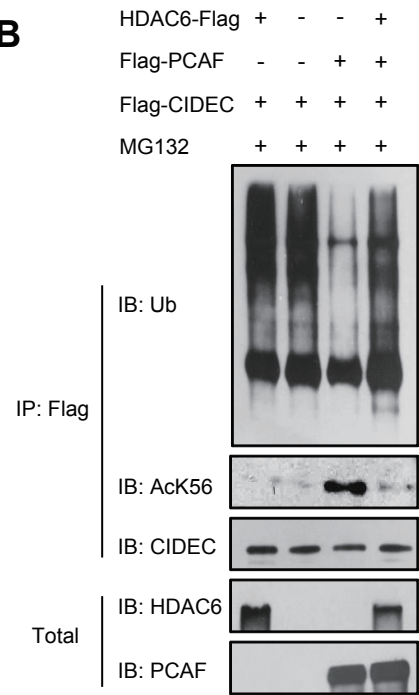**Supplemental Figure 3. Related to Figure 3. Lysine 56 is the acetylation site of CIDEC.**

(**A**) Catalytic activity of PCAF is required for CIDEC acetylation. 568/569/570-A represents PCAF harboring the triple a.a mutations that disrupt its enzymatic activity. Data represent results from at least 3 independent experiments.

(**B**) The HDAC6-selective inhibitor, Tubacin, enhances CIDEC acetylation. 293T cells were treated with 5 mM Tubacin or 5 mM NaB for 12 hrs. Data represent results from at least 3 independent experiments.

(**C**) Identification of acetylated peptides on CIDEC by mass spectrometry.

(**D**) Mutations at Lysine 34 and 56 decreased CIDEC acetylation. Flag-tagged wild-type CIDEC (WT) or its various mutaions (K34/56R, K75/77/79R, K115/117R, K134/137/138R and K150/226R) were co-expressed with PCAF in 293T cells and the immuno-precipitated with antibodies against Flag. Levels of their acetylation were detected with antibodies against acetylated lysine residue. Data represent results from at least 3 independent experiments.

(**E**) Spectra of acetylated K34 containing CIDEC peptides. Acetylated lysine residue is colored in red and also denoted by an asterisk.

(**F**) Spectra of acetylated K56 containing CIDEC peptides. Acetylated lysine residue is colored in red and also denoted by an asterisk.

(**G**) Mutation of lysine 56 to arginine (K56R) decreases CIDEC acetylation. Data represent results from at least 3 independent experiments.

(**H**) The acetylation defective form of CIDEC K56R cannot be acetylated in vitro. Data represent results from at least 3 independent experiments.

(**I**) Knockdown HDAC6 increases CIDEC acetylation in 3T3-L1 adipocyte. Data represent results from at least 3 independent experiments.
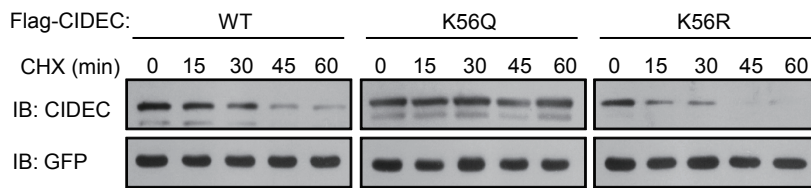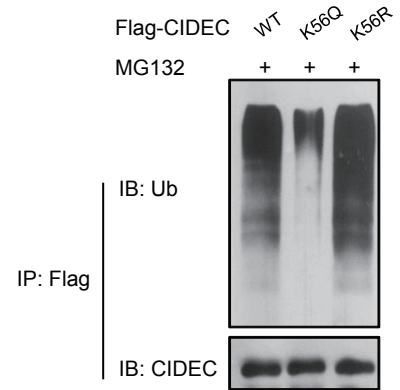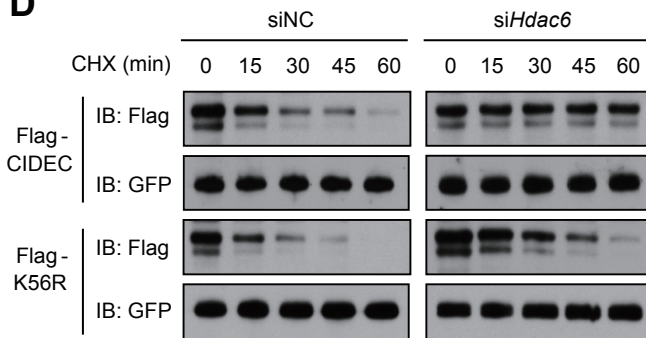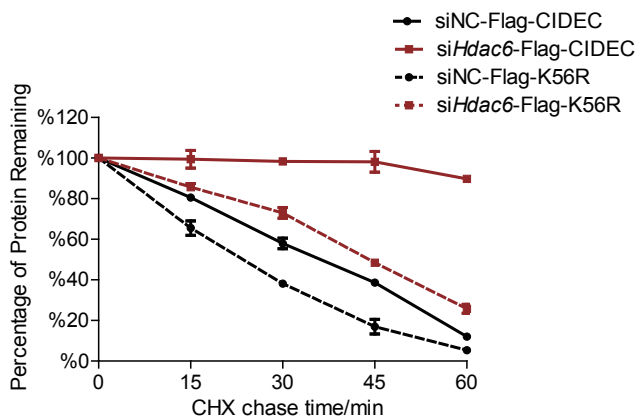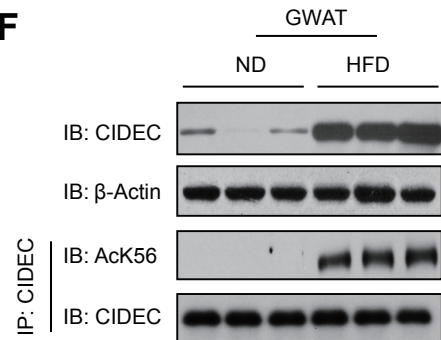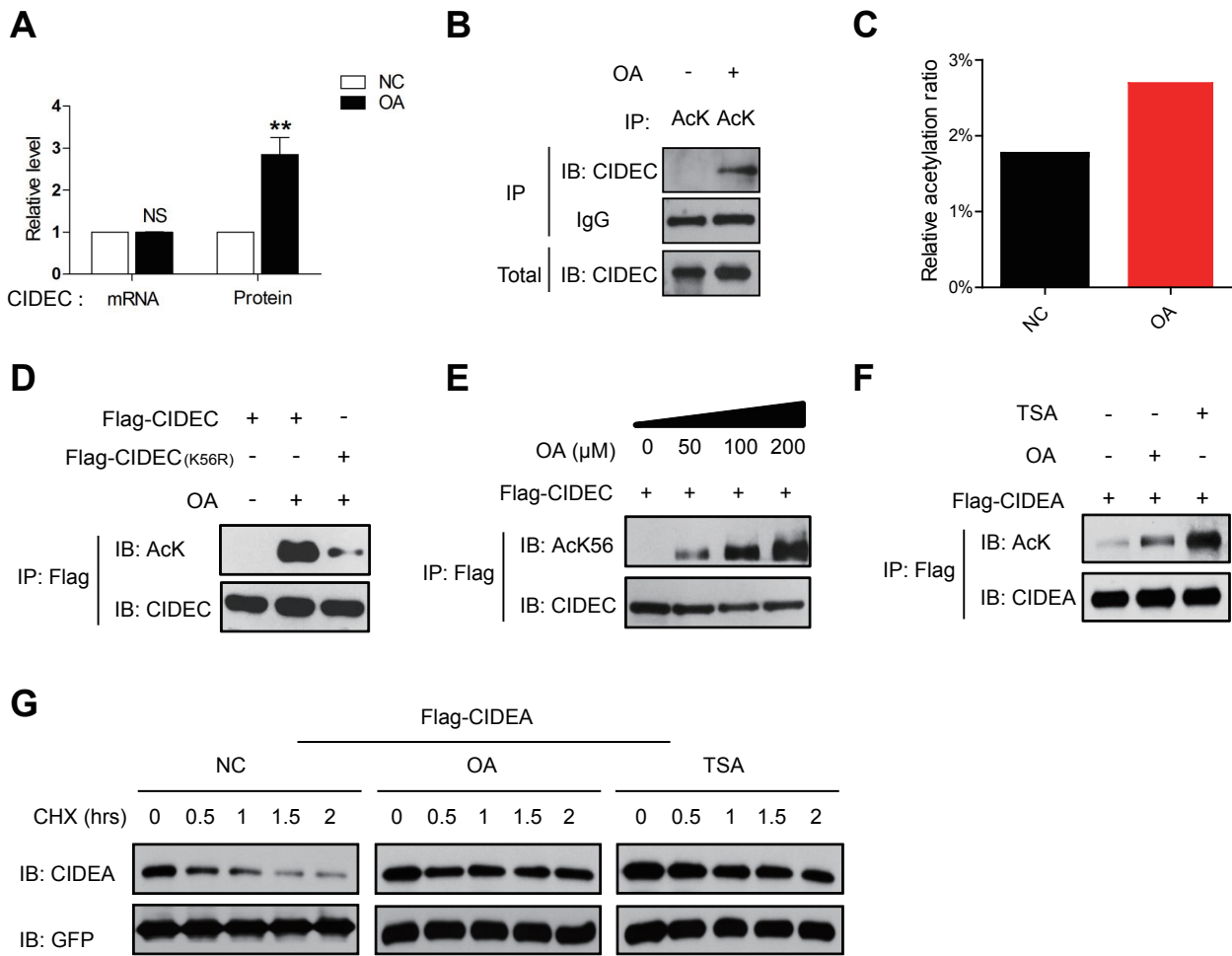
Supplemental Figure 4

Supplemental Figure 4. Related to Figure 4. Acetylation of CIDEC increases its stability.

(**A**) HDAC6 decreased the stability of ectopically expressed CIDEC in 293T cells while PCAF increased its stability. Two-way repeated-measurement analysis of variance (ANOVA) with Holm-Sidak post-hoc test was used. Statistical difference was indicated as [###]$P < 0.001$. Data represent results from at least 3 independent experiments.

(**B**) HDAC6 increased the levels of CIDEC ubiquitination. Data represent results from at least 3 independent experiments.

(**C**) Acetylation-mimicking form (K56Q) of CIDEC has increased stability. Data represent results from at least 3 independent experiments.

(**D**) The stability of Flag-tagged-CIDEC and K56R in 293T cells that were transfected with scramble siRNA (control) and in 293T cells transfected with *Hdac6* specific siRNA. Data represent results from 3 independent experiments.

(**E**) Acetylation-mimicking mutant (K56Q) but not the acetylation defective mutant (K56R) of CIDEC has decreased ubiquitination. Data represent results from at least 3 independent experiments.

(**F**) Levels of CIDEC protein and acetylated form were both increased in High-fat-diet (HFD) fed mice. Immunoprecipited CIDEC was normalized and used as loading control for acetylation measurement (n=3 mice per group).
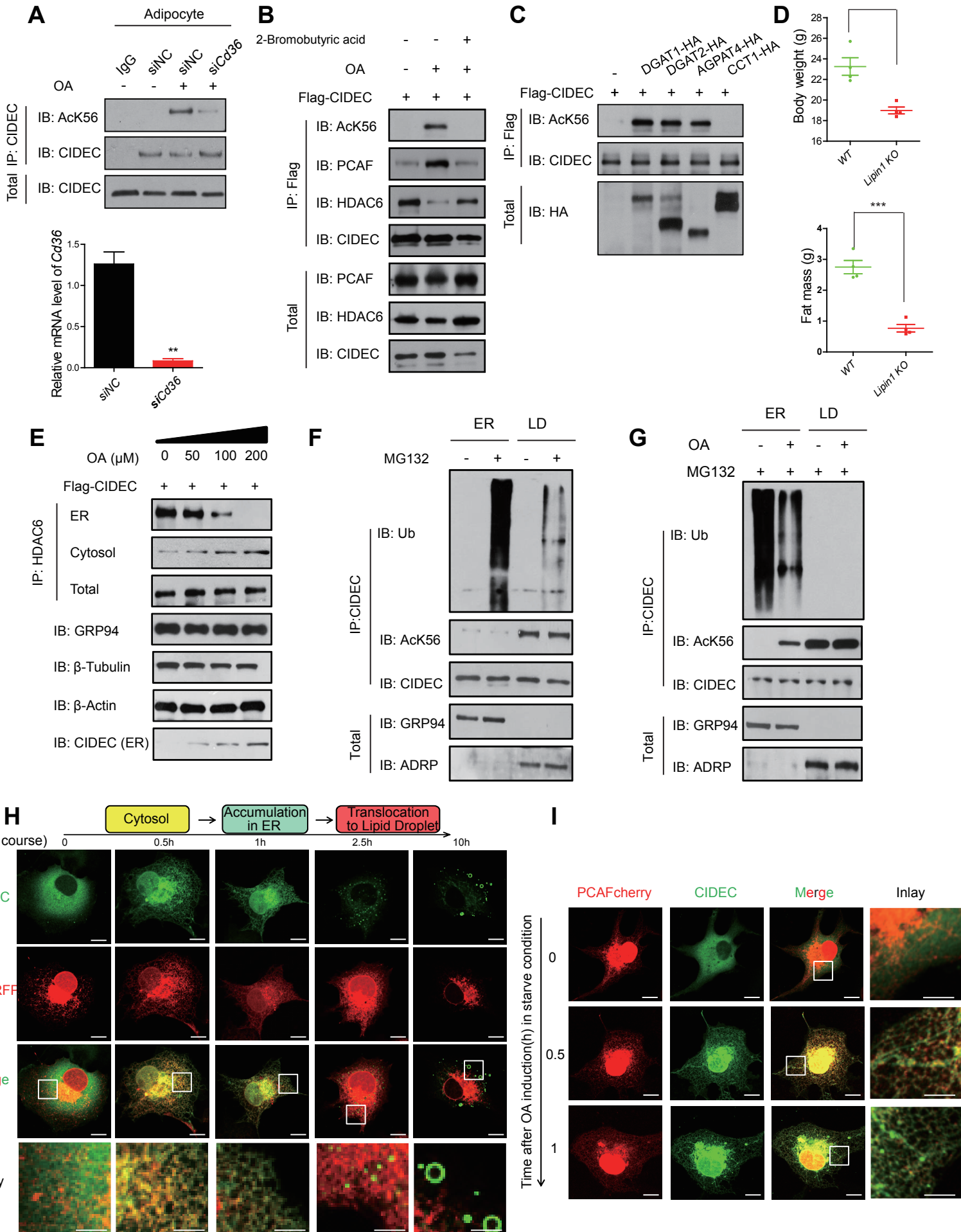
Supplemental Figure 5

A

B

C

D

E

F

G

Supplemental Figure 5. Related to Figure 6. FAs enhance the stability and acetylation of CIDEC and CIDEA.

(**A**) Relative levels of CIDEC protein were increased in the presence of OA (n=3 samples per group). Data represent the mean ± SEM. Statistical difference was indicated as *P < 0.05, **P < 0.01, ***P < 0.001, by two-tailed Student's t test.

(**B**) OA induced CIDEC acetylation in 3T3-L1 adipocytes. Cells were treatment with 200 μM OA. Data represent results from at least 3 independent experiments.

(**C**) Relative ratio of acetylated CIDEC at K56 that was expressed in 293T cells in the absence (NC) or presence of OA.

(**D**) CIDEC K56R had lower acetylation in the presence of OA. Data represent results from at least 3 independent experiments.

(**E**) OA induced CIDEC acetylation in a dose dependent manner. 293T cells transfected with Flag-CIDEC were treatment with OA for the indicated concentrations. Data represent results from at least 3 independent experiments.

(**F**) OA and TSA increased CIDEA acetylation. Acetylated CIDEA was detected in the immunoprecipitated product using antibody against acetylated lysine (AcK). Data represent results from at least 3 independent experiments.

(**G**) OA and TSA increased the stability of CIDEA. Data represent results from at least 3 independent experiments.

Supplemental Figure 6

Supplemental Figure 6. Related to Figure 7. TAG synthesis in the ER controls the dynamic association between HDAC6, CIDEC and PCAF.
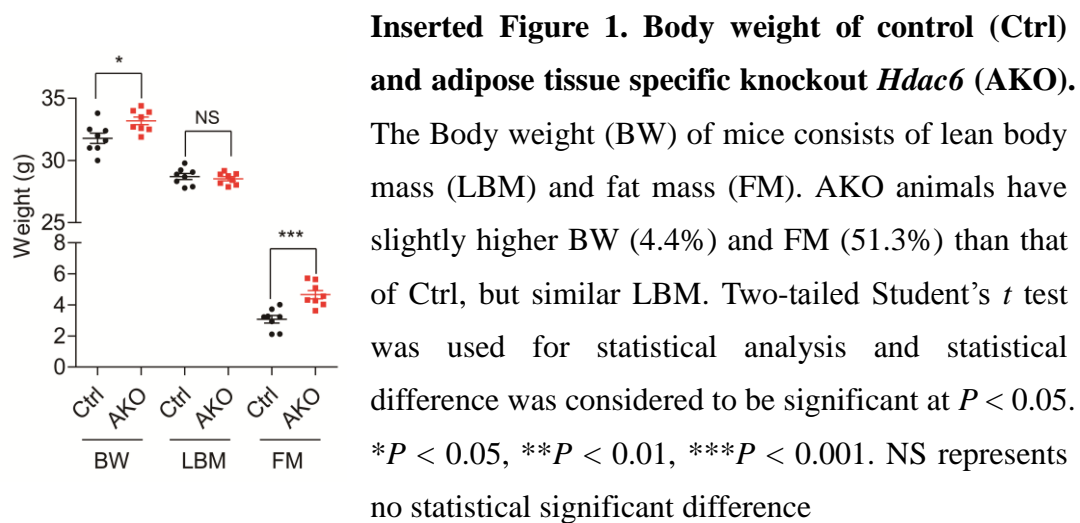
(**A**) Knocking down *Cd36* inhibited CIDEC acetylation. Data represent results from 3 independent experiments.

(**B**) FA-induced dynamic interaction between CIDEC, PCAF and HDAC6 was depended on DGAT activity. Data represent results from 3 independent experiments.

(**C**) Overexpression of enzymes in TAG synthesis pathways increased CIDEC acetylation. Data represent results from at least 3 independent experiments.

(**D**) The body weight and fat mass from *Lipin1* deficient mice were lower than that of wild-type mice (n=4 mice per group).

(**E**) Levels of HDAC6 in various biochemical fractions in the presence of increasing amount of OA. Data represent results from at least 3 independent experiments.

(**F**) ER-associated CIDEC was ubiquitinated. CIDEC protein from the ER and LD fractions of 293T cells treated with MG132 were immuno-precipitated. Levels of ubiquitinated CIDEC were detected using antibodies against ubiquitin. Data represent results from at least 3 independent experiments.

(**G**) OA inhibited the ubiquitinaiton of CIDEC in the ER fraction. Data represent results from at least 3 independent experiments.

(**H**) Representative images showing the subcellular localization of CIDEC in the presence or absence of OA. Scale bars represent 5 μm and 2 μm (insets), respectively. Data represent results from at least 5 independent experiments.

(**I**) Representative images showing the co-localization between PCAF (Red) and CIDEC (green) in the absence of OA. Scale bars represent 5 μm and 2 μm (insets), respectively. Data represent results from at least 5 independent experiments.

Data represent the mean $\pm$ SEM. Statistical difference was indicated as *$P < 0.05$, **$P < 0.01$, ***$P < 0.001$, by two-tailed Student's *t* test.

Supplemental Experimental Procedures

Statistical analyses for comparison of oxygen consumption-

We used three different statistical methods to evaluate the relationship of oxygen (O_2) consumption to total body weight (BW), lean body mass (LBM) or fat mass (FM) between animals of control (Ctrl) and adipose-specific knockout of *Hdac6* (AKO). These methods include 1) **a direct comparison method**; 2) **ratio-based method;** and 3) **the analysis of co-variance (ANCOVA) using a multiple linear regression model**. Before we go through in detail of the statistical analyses, we would like to emphasize that we used 8 pairs of age-matched (three months old) and gender-matched (male) control or AKO mice for our analysis in oxygen consumption. Such method is commonly used to evaluate the correlation of oxygen consumption and their genetic background (1-11). As shown in Inserted Figure 1, AKO mice had slightly higher body weight (approximately 4.4% heavier than control mice), similar lean body mass (LBM) but significantly higher fat mass (FM) compared with control mice (approximately 51.3% heavier than control mice).

Inserted Figure 1. Body weight of control (Ctrl) and adipose tissue specific knockout *Hdac6* (AKO). The Body weight (BW) of mice consists of lean body mass (LBM) and fat mass (FM). AKO animals have slightly higher BW (4.4%) and FM (51.3%) than that of Ctrl, but similar LBM. Two-tailed Student's *t* test was used for statistical analysis and statistical difference was considered to be significant at $P < 0.05$. *$P < 0.05$, **$P < 0.01$, ***$P < 0.001$. NS represents no statistical significant difference

In a direct comparison method, taking advantage of the small difference in BW between control and AKO mice, we directly compared the O_2 consumption between Ctrl and AKO mice by using two-tailed Student's *t* test. Similar approach has been used in many references (1-4) including recent papers from JCI (3, 4). As shown in Inserted Table 1, **the O_2 consumption in AKO animals is significantly lower than that of control (Ctrl) mice under dark cycle ($P = 0.0199$)**. These results are reported in Figure 2A.

Inserted Table 1. Comparison of Oxygen (O$_2$) consumption of control (Ctrl) and adipose tissue specific knockout *Hdac6* (AKO) mice by using the direct comparison method.

Parameters	Dark		Light	
	Ctrl (n = 8)	AKO (n = 8)	Ctrl (n = 8)	AKO (n = 8)
O$_2$ consumption[1] (VO$_2$, ml/min)	1.93 ±0.15	1.74 ±0.14[*]	1.47 ±0.13	1.55 ±0.09

[1]Mean ±SD

[*]P <0.05, by two-tailed Student's *t* test.

In the ratio-based method, we normalized the O$_2$ consumption rate by calculating the ratio of O$_2$ consumption to their corresponding BW or LBM in control (Ctrl) and AKO mice. Similar method has also been frequently used by many scientists (5-11). Consistent with the direct comparison method, we observed significantly reduced **O$_2$ consumption in the AKO mice under the dark cycle (P = 0.003 in the BW-ratio method and P = 0.029 in the LBM-ratio method)** (Inserted Table 2). These data are reported in Supplementary Figure 2A.

Inserted Table 2. Comparison of Oxygen (O$_2$) consumption of control (Ctrl) and adipose tissue specific knockout *Hdac6* (AKO) mice by using the ratio-based method.

| Parameters	Dark		Light	
	Ctrl (n = 8)	AKO (n = 8)	Ctrl (n = 8)	AKO (n = 8)
BW-Ratio VO$_2$ (ml.min^{-1}. g^{-1})[1]	0.061 ±0.005	0.053 ±0.005[**]	0.046 ±0.004	0.047 ±0.003
LBM-Ratio VO$_2$ (ml.min^{-1}. g^{-1})[1]	0.067 ±0.005	0.061 ±0.005[*]	0.051 ±0.004	0.054 ±0.003

[1]Mean ±SD

[*]P <0.05, [**]P < 0.01, by two-tailed Student's *t* test.

Most importantly, we have conducted ANCOVA according to the descriptions by Kaiyala and others (12-17). We created a multiple linear regression model to

investigate the correlation of O_2 consumption with the body weights of these two genotypes. The model includes genotype, lean body mass (LBM), and fat mass (FM). As you can see in the Inserted Figure 2, statistical analysis using the regression model suggests that there are small correlation coefficients R^2 of O_2 consumption with LBM and FM in Ctrl ($R^2 = 0.021$, $P = 0.949$) and in AKO mice ($R^2 = 0.034$, $P = 0.916$) (Inserted Figure 2). The regression equations are as follows:

$$[VO_2 \text{ (ml/min)} = 1.51 + 0.012 \text{ (LBM, g)} + 0.025 \text{ (FM, g)}] \qquad \text{(Ctrl)}$$

$$[VO_2 \text{ (ml/min)} = 0.96 + 0.022 \text{ (LBM, g)} + 0.031 \text{ (FM, g)}] \qquad \text{(AKO)}$$
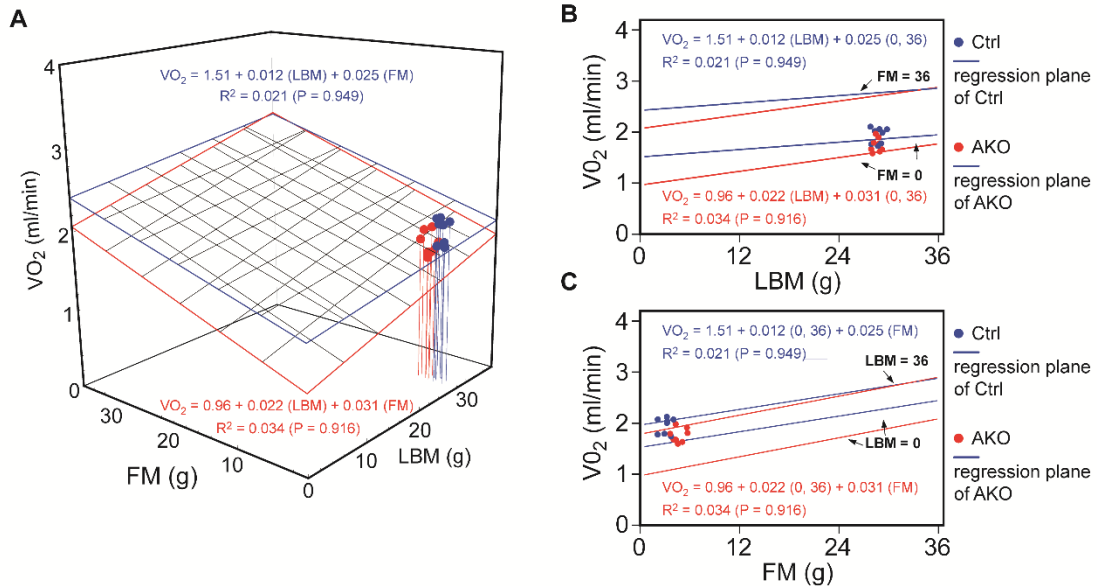
Inserted Figure 2. Multiple linear regression model for coefficient estimates of oxygen consumption (VO_2) to lean body mass (LBM) and fat mass (FM) in the control (blue) and the AKO mice (red) under dark cycle (A). (B-C) The projections of the relationship of O_2 consumptions to LBM and FM from the panel (A), respectively. All estimated correlation coefficients are too small with $P > 0.05$ in the linear regression. R^2, correlation coefficient.

We think the low correlations may result from the narrow distribution of BW as we conducted our experiments using animals at specific age (three months old) and collected their oxygen consumption data within 72 hours, an approach used by other scientists in the field. Indeed, we calculated their coefficients of variances (CVs) and observed that the corresponding CVs of BW were 3.65% for Ctrl (1.16 g/ 31.79 g) and 2.65% for AKO (0.88 g/ 33.19 g), respectively. A small CV value represents a

narrow dispersion of BW (Inserted Figures 1 and 2).

By contrast, wide distribution of BW was observed in other studies (15-17). Therefore, the ANCOVA was likely feasible to evaluate the correlation of oxygen consumption with LBM and FM of animals with wide distribution of BW. But the ANCOVA may not be suitable for our comparison of oxygen consumption of laboratory animals that are at specific age with narrow BW distribution.

Interestingly, we observed that according to the regression planes of O_2 consumption for the Ctrl and the AKO (Inserted Figure 2), the regressed O_2 consumption of the Ctrl mice is always higher than that of the AKO mice within the range of BW examined. Despite **the potential statistical risk** of ANCOVA, we went ahead and calculated the regression-adjusted O_2 consumption of these two genotypes and observed that **the regression-adjusted oxygen consumption is significantly lower for AKO mice (P = 0.006,** Inserted Table 3). These data are reported in Supplementary Figure 2B.

Inserted Table 3. Comparison of Oxygen (O_2) consumptions of control (Ctrl) and adipose tissue specific knockout *Hdac6* (AKO) mice by using the analysis of co-variance (ANCOVA).

Parameters	Dark		Light	
	Ctrl (n = 8)	AKO (n = 8)	Ctrl (n = 8)	AKO (n = 8)
Regression-adjusted VO_2 (ml/min)[1]	1.95 ±0.15	1.72 ±0.14[**]	1.51 ±0.13	1.53 ±0.09

[1]Mean ±SD

[**]$P < 0.01$, by two-tailed Student's *t* test.

In summary, we used three different statistical methods that have been used by scientists in the field to address the difference of oxygen consumption in the Ctrl and AKO mice. These three methods all reached to similar conclusion that **the O_2 consumption of the AKO mice is significantly lower than that of the Ctrl mice at dark cycle when the animals are metabolically active. We think each method has its limitation and multiple analyses are probably required to draw the correct conclusion for multiple comparisons.**

Supplemental References

1.   Lee MW, Odegaard JI, Mukundan L, Qiu Y, Molofsky AB, Nussbaum JC, Yun K, Locksley RM, and Chawla A. Activated type 2 innate lymphoid cells regulate beige fat biogenesis. *Cell.* 2015;160(1-2):74-87.

2.   Qiu Y, Nguyen KD, Odegaard JI, Cui X, Tian X, Locksley RM, Palmiter RD, and Chawla A. Eosinophils and type 2 cytokine signaling in macrophages orchestrate development of functional beige fat. *Cell.* 2014;157(6):1292-308.

3.   Maida A, Zota A, Sjoberg KA, Schumacher J, Sijmonsma TP, Pfenninger A, Christensen MM, Gantert T, Fuhrmeister J, Rothermel U, et al. A liver stress-endocrine nexus promotes metabolic integrity during dietary protein dilution. *J Clin Invest.* 2016;126(9):3263-78.

4.   Kumari M, Wang X, Lantier L, Lyubetskaya A, Eguchi J, Kang S, Tenen D, Roh HC, Kong X, Kazak L, et al. IRF3 promotes adipose inflammation and insulin resistance and represses browning. *J Clin Invest.* 2016;126(8):2839-54.

5.   Zhu Q, Ghoshal S, Rodrigues A, Gao S, Asterian A, Kamenecka TM, Barrow JC, and Chakraborty A. Adipocyte-specific deletion of Ip6k1 reduces diet-induced obesity by enhancing AMPK-mediated thermogenesis. *J Clin Invest.* 2016;126(11):4273-88.

6.   Winnay JN, Solheim MH, Dirice E, Sakaguchi M, Noh HL, Kang HJ, Takahashi H, Chudasama KK, Kim JK, Molven A, et al. PI3-kinase mutation linked to insulin and growth factor resistance in vivo. *J Clin Invest.* 2016;126(4):1401-12.

7.   Chen M, Shrestha YB, Podyma B, Cui Z, Naglieri B, Sun H, Ho T, Wilson EA, Li YQ, Gavrilova O, et al. Gsalpha deficiency in the dorsomedial hypothalamus underlies obesity associated with Gsalpha mutations. *J Clin Invest.* 2016.

8.   Dodd GT, Decherf S, Loh K, Simonds SE, Wiede F, Balland E, Merry TL, Munzberg H, Zhang ZY, Kahn BB, et al. Leptin and insulin act on POMC neurons to promote the browning of white fat. *Cell.* 2015;160(1-2):88-104.

9.   Rao RR, Long JZ, White JP, Svensson KJ, Lou J, Lokurkar I, Jedrychowski MP, Ruas JL, Wrann CD, Lo JC, et al. Meteorin-like is a hormone that regulates immune-adipose interactions to increase beige fat thermogenesis. *Cell.* 2014;157(6):1279-91.

10. Chaurasia B, Kaddai VA, Lancaster GI, Henstridge DC, Sriram S, Galam DL, Gopalan V, Prakash KN, Velan SS, Bulchand S, et al. Adipocyte Ceramides Regulate Subcutaneous Adipose Browning, Inflammation, and Metabolism. *Cell Metab.* 2016;24(6):820-34.

11. Wang H, Liu L, Lin JZ, Aprahamian TR, and Farmer SR. Browning of White

Adipose Tissue with Roscovitine Induces a Distinct Population of UCP1+ Adipocytes. *Cell Metab.* 2016;24(6):835-47.

12. Kaiyala KJ, and Schwartz MW. Toward a more complete (and less controversial) understanding of energy expenditure and its role in obesity pathogenesis. *Diabetes.* 2011;60(1):17-23.

13. Kaiyala KJ, Morton GJ, Leroux BG, Ogimoto K, Wisse B, and Schwartz MW. Identification of body fat mass as a major determinant of metabolic rate in mice. *Diabetes.* 2010;59(7):1657-66.

14. Wyatt HR, Grunwald GK, Seagle HM, Klem ML, McGuire MT, Wing RR, and Hill JO. Resting energy expenditure in reduced-obese subjects in the National Weight Control Registry. *Am J Clin Nutr.* 1999;69(6):1189-93.

15. Bitz C, Toubro S, Larsen TM, Harder H, Rennie KL, Jebb SA, and Astrup A. Increased 24-h energy expenditure in type 2 diabetes. *Diabetes Care.* 2004;27(10):2416-21.

16. Poehlman ET, and Toth MJ. Mathematical ratios lead to spurious conclusions regarding age- and sex-related differences in resting metabolic rate. *Am J Clin Nutr.* 1995;61(3):482-5.

17. Nelson KM, Weinsier RL, Long CL, and Schutz Y. Prediction of resting energy expenditure from fat-free mass and fat mass. *Am J Clin Nutr.* 1992;56(5):848-56.

Supplemental experimental procedures

Supplemental methods

Plasmids construction, antibodies, reagents and recombinant protein

HDAC1-Flag, HDAC2-HA, HDAC3-Flag, HDAC4-Flag, HDAC6-Flag, HDAC7-Flag, HDAC10–Flag, Tip60-Flag constructs were gifts from Dr. S.C. Lin (Xiamen University, Xiamen, China). P300, CBP-HA, PCAF-Flag, GCN5-Myc, Sirt1-HA constructs were gifts from Dr. S.M. Zhao (FuDan University, Shanghai, China). The shRNA expression plasmid against human DGAT1 and DGAT2 were purchased from Sigma-Aldrich (USA). The expression constructs of CIDEC were as previously described (1). Point mutations of CIDEC and PCAF were generated by a PCR-based site-directed mutagenesis method (Stratagene). The accuracy of each plasmid DNAs was verified by sequencing analysis.

Antibodies of HDAC2, HDAC3, HDAC4 and HDAC7 were gifts from Dr. S.C. Lin (Xiamen University, Xiamen, China). Antibody against the globular domain of ADIPONECTIN was a gift from Dr Z. Li (Tsinghua University, Beijing, China). Antibodies such as mouse anti-HA (sc-7392), rabbit anti-FLAG (sc-807), GFP (sc-8334), MBP (sc-13564), HDAC1 (sc-7872), HDAC8 (sc-11405), HDAC9 (sc-28732), TIP47 (sc-14726R), DGAT1 (sc-26173), DGAT2 (sc-32400), Ub (sc-8017), GRP94 (sc-32249), protein A/G beads (sc-2003) and normal mouse or rabbit IgG (sc-2025 & sc-2027) were purchased from Santa Cruz Biotechnology (USA). Acetylated-Lysine antibody (#9441), PCAF (#3378), HDAC6 (#7558), α-Tubulin (#2125), CPT1 (#12252), LIPIN1 (#5195) and FABP4 (#3544) were purchased from Cell Signaling Technology (USA). Antibodies against human CIDEC (ab77115), CPT2 (ab181114), COX4 (ab202554), ADIPONECTIN (ab22554) and acetylation α-Tubulin (Ac-αTub) (ab179484) were purchased from Abcam (UK) and UCP1 (662045) was from Calbiochem (Germany). Antibodies against ADRP (20R-Ap002) and PLIN1 (20R-pp004) were purchased from Fitzgerald Industries (USA) and GST (AB101) was from Tiangen (China). Cytochrome C antibody (556433) was purchased from Pharmingen (USA). Antibodies against β-Actin

(A5441), β-Tubulin (T0198), CNX (C4731), mouse anti-FLAG (F1804) and anti-FLAG M2 agarose beads (A2220) were purchased from Sigma-Aldrich (USA). Western blots were developed using HRP-conjugated anti-mouse (NA-931), anti-rabbit (NA-934) second antibodies from GE Healthcare (USA), anti-rat (112-035-003) from Jackson InmmunoResearch (USA), anti-guinea pig (6090-05) from Southern Biotech (USA), and anti-rabbit without recognition of heavy and light chains (18-8816-31) from Rockland (USA). The rabbit polyclonal antibodies against mouse CIDEA, CIDEB and CIDEC were generated by the injection of rabbits with His-tagged truncated mouse CIDEA (aa 1-195), mouse CIDEB (aa 1-176) and mouse CIDEC (aa 1-190) recombinant proteins that were expressed in and purified in *Escherichia coli* (2, 3). The generation of CIDEC K56-specific acetylated antibody was made by Genomics technology (Shanghai, China). MBP-CIDEC protein was a gift from Dr. Y.A. Yuan (National University of Singapore, Singapore). PCAF (a.a. 352-832) recombinant GST fusion protein was purchased from Millipore (Darmstadt, Germany). Recombinant protein for HDAC6-GST was purchased from Cayman (Michigan, USA).

Cell culture, treatment and transfection

293T cells, 3T3-L1 pre-adipocytes and Cos7 cell were cultured in DMEM (Invitrogen) containing 10% FBS (Invitrogen), 2mM L-glutamine, 100U/ml penicillin and 100μg/ml streptomycin at 37℃ in a humidified incubator containing 5% CO_2. Monolayers of 3T3-L1 pre-adipocytes were induced to differentiate into mature adipocytes as previously described (4) . To promote the formation of LDs, cells were treated with Oleic acid or other fatty acids conjugated to fatty acid–free BSA at a molar ratio of 6:1 and added to the culture medium to give a final concentration of 200μM/L (unless other concentration is specified). TSA (0.5μM) and NAM (5mM) were added to the culture medium 6 h before cell harvest. 293T cells were treated by 5mM tubacin, or 5mM NaB for 12 hr. Glucose-free medium was prepared with DMEM base (GIBCO) and supplemented with 50mM glucose (Sigma). Glucose

treatment was carried out by culturing cells in DMEM medium for 24hr before the desired medium was used to replace DMEM medium.

Plasmid DNAs were transfected into 293T cells and 3T3-L1 pre-adipocytes using Lipofectamine 2000 according to manufacturer's instruction (Invitrogen), Electroporation of 3T3-L1 pre-adipocyte and mature adipocyte were performed on Amaxa Nucleofector II (Lonza) with program A-033 according to the manufacturer's instruction.

Protein stability assay

CIDEC and CIDEA stability assay in 293T cells or 3T3-L1 adipocytes was measured using a CHX-based protein-chase experiment. For 293T cells, expression plasmids encoding Flag-CIDEC, Flag-CIDEA, CIDEC mutations were transfected using the calcium phosphate method. 24 hours post-transfection, the medium was replaced with fresh Dulbecco's modified Eagle's medium plus 10% fetal bovine serum, followed by the addition of CHX ($100\,\mu g/ml$) and harvested at different time points after CHX was added. To determine the stability of endogenous CIDEC in 3T3-L1 adipocytes, 8 days differentiated cells were treated with CHX and harvested the same manner with the 293T cells. For quantitative analysis, the Western blot bands were scanned and further quantified using Quantity One software (Bio-Rad).

Immunoprecipitation and western blotting

Immunoprecipitation was carried out as described previously (5). For immunoprecipitation of endogenous proteins, 8-day differentiated 3T3-L1 adipocytes or adipose tissue in mice, monkey and human were collected and lysed in IP buffer (20mM Tris, pH7.4, 150mM NaCl, 1% Triton X-100) by sonication. Antibodies against CIDEC, PCAF, HDAC6 or pre-immune serum were conjugated to protein A/G beads and used for immunoprecipitation. Western blotting was blocked with 5% fat-free milk. Acetylation western blotting was blocked with peptone buffer [50mM Tris (pH 7.5) with 10% (V/V) Tween-20 and 1% peptone (AMRESCO)] while 50mM

Tris (pH 7.5) with 0.1% peptone was used to prepare primary and secondary antibodies.

Ubiquitin conjugation assay

293T cells were transfected with Plasmids using the calcium phosphate co-precipitation technique. 24 hours post-transfection, the cells were treated with 10 μM MG132 for 6h or untreated and then harvested and sonicated in IP buffer. The diluted samples were used for immunoprecipitation with M2 beads conjugated with a FLAG-specific antibody (Sigma). Immunoprecipitates or total cell lysates were subjected to SDS-PAGE and Western blot analysis. In experiments based on 3T3-L1 adipocytes, endogenous CIDEC was immunoprecipitated using an antibody against CIDEC.

Immunofluorescent staining

Procedures for immunofluorescent staining were similar as previously described(2). For fatty acid free condition, procedures were followed according to protocols as previously published (6). Starvation was performed by culturing cells in DMEM, L-glutamine, pyruvate, and nonessential amino acids but in the absence of serum for 24hr. To promote the formation of LDs, cells were treated with oleic acid conjugated to fatty acid-free BSA at a molar ratio of 6:1 and added to the culture medium to give a final concentration of 200μM (unless other concentration is specified). Then cells were rinsed twice in PBS, fixed with 4% PFA for 20min, permeabilized with 0.4% TritonX-100 in PBS for 20min, blocked with 10% goat serum in PBS for 1hr, followed by incubation with primary antibody for 2hr, washed three times with PBS, and incubated with fluorescently labeled secondary antibody (1:500 dilution) for 1hr followed by Hoechst and/or BODIPY, as indicated. Coverslips were mounted after three times washing with PBS. Images for protein localization were acquired under an LSM710 confocal microscope (Carl Zeiss) with 63×oil immersion objective.

Measurement of LD sizes

Quantitative analysis of LD size in 3T3-L1 pre-adipocytes or adipocytes was described by Sun et al (1). For quantitative analysis of cells containing large LDs, plasmids DNA or siRNAs were introduced into cells and incubated with 200 μM oleic acid complexed to albumin for 18hr, fixed, and stained with Bodipy 493/503. The percentage of cells containing at least one LD larger than 2.0 μm in diameter was calculated and approximately 150 cells from three independent experiments were analyzed. To measure the LD size in 3T3-L1 differentiate adipocytes, the diameter of largest LD in one cells were calculated after introducing indicated siRNAs, fixed and stained with Bodipy 493/503. At least 200 cells were analyzed in each condition. Image were obtained under an inverted microscope Axiovert 200M (Carl Zeiss) or LSM710 confocal microscope (Carl Zeiss).

Measurement of neutral lipid transfer rates under DIC imaging

For live cell imaging, showing neutral lipid transfer processes from small (donor) lipid droplets (LDs) to large (acceptor) lipid droplets, CIDEC-GFP were overexpressed with indicated proteins in 3T3-L1 pre-adipocytes. Cells were incubated in coverglass-bottom dishes for inspection via a microscope. Differential interference contrast (DIC) images were acquired under an inverted confocal microscope (A1Rsi, Nikon, Japan) with a 100× oil-immersed objective. The initial diameters of accepter LDs and donor LDs were selected nearly at 3.0μm ± 0.5μm and 2.0μm ± 0.5μm, respectively. Acquisition was controlled under a NIS program (Nikon). Time-lapse videos were collected at 37 ℃ with a 2-min interval over 2–4 h. Every sequence of time-lapse 1024×1024 pixels images was stacked into a NIS-associated format (*.nd2) for next image processing.

Lipid transfer rates were calculated as previously described (Gong et al., 2011) with some modifications. In brief, the initial diameter of a donor LD was measured from the first five frames of DIC images and was calculated as an average. A lipid transfer rate, under an assumption of a spherical LD, could be calculated by dividing the initial volume of the donor LD with the duration of the lipid transfer process. Almost every

15 independent lipid transfer events in cells individually expressing wild-type CIDEC, K56R-mutant CIDEC, and K56Q-mutant CIDEC with or without oleic acid were acquired. Lipid transfer rates were statistically estimated and plotted in figures accordingly.

FRAP-based lipid exchange assay

3T3-L1 pre-adipocytes transfected with indicated plasmids (wild-type CIDEC, K56R-mutant CIDEC, and K56Q-mutant CIDEC) were incubated with 200mM oleic acid and 1mg/ml Bodipy 558/568 C12 fatty acid (Molecular Probes) for 18hr and then were changed to fresh medium 1hr before FRAP experiments. For 3T3-L1 adipocyte, 8-days differentiated cells were electroporated with indicated siRNAs and incubated with Bodipy 558/568 C12 fatty acid (Molecular Probes), the same treatment with pre-adipocytes. Live cells were viewed under a confocal microscope (LSM710, Carl Zeiss) using a $63\times$ oil-immersed objective. LD pairs with a range of diameter between 4μm and 6μm and with a clear green fluorescent signal at LDCS were selected for bleaching. Selected regions were bleached 500 interactions by 100% laser power (543 nm diode laser), followed by time-lapse scanning with a 12.5s interval. Mean optical intensity (MOI) within LD core regions were measured simultaneously. Approximately 20 pairs of LDs were analyzed in each experiment. Digital gain and laser power were set to avoid overexposure to ensure accurate quantification of fluorescence.

Calculation of lipid exchange rates was essentially the same as previously described (1, 5). The mean optical intensity (MOI) of both bleached and unbleached LD was measured with ZEN 2009. To obtain fluorescence recovery curves, MOI values were calculated as the percentage of the original fluorescent intensity and plotted by using Prism 5.

Image processing

All frames in every time-lapse or FRAP experiments were adjusted in parallel to a

similar brightness level or contrast through ImageJ (NIH). Modified images were exported out in 24-bit RGB TIFF format. Also, further image processing, such as enlarging certain region as a panel, movies exporting, and time stamps, was performed in ImageJ. Time-lapse movies, including original frames of 1024×1024 pixels and enlargements of 500×500 pixels, were exported out in 24-bit RGB AVI format via ImageJ with a rate of 30 frames per second for making custom-made picture-in-picture (PIP) movies. The PIP movies were finally made by downsizing original frames, docking them into the relevant enlargements, and exporting them out in GIF format with 500×500 pixels by using Camtasia Studio version 6 (TechSmith Corp, USA).

Human intra-abdominal fat specimens

The human intra-abdominal fat specimens were divided into two categories (normal and obese) according to BMI of the patients. The normal intra-abdominal fat samples were collected from Air Force General Hospital, PLA and the obese fat samples were collected by Shanghai Sixth People's Hospital. The morphology of these fat specimens was examined by electron microscopy (semi-thin sections, 0.5μm).

Rhesus monkey visceral fat specimens

The Rhesus monkey visceral fat specimens were collected from male adult rhesus monkeys from three NHP facilities: the Academic of Military Medical Science (AMMS), Beijing (n=60); Fangshan Breeding Facility, Institute of Beijing Xieer'xin Biology Resource, Beijing (920653); and Guangxi Grandforest Scientific Primate Co., Ltd., Guangxi, China (950805, 921101, 950723, 950607) and Chengdu (99013). Tissues of rhesus monkeys (*Macaca mulatta*) were obtained from nonhuman primate research center, institute of molecular medicine, Peking University. The detail information of these samples was listed:

99013, age: 13.8 years; bodyweight: 8.14kg

920653, age: 19.8 years; bodyweight: 8.24kg

921101, age: 18.9 years; bodyweight: 12.42kg

950805, age: 15.7 years; bodyweight: 22.3kg

950607, age: 14.9 years; bodyweight: 20.7kg

950723, age: 15.2 years; bodyweight: 20.1kg

The body weight of the rhesus monkey greater than or equal to 15kg was considered as obesity.

Adiposity index, histological analysis and blood chemistry

Procedures for adiposity index, electron microscopy, histological analysis and blood chemistry were essentially the same as previously described (Zhou et al., 2003). For adiposity index analysis, we dissected gonadal, mesenteric, retroperitoneal, subcutaneous fat pads from control and *Hdac6* adipose tissue specific knockout mice according to various anatomical landmarks, and weighed them. We calculated adiposity index as the total weight of white fat pads from these locations divided by the total body weight.

The fat tissues from control and *Hdac6* adipose tissue specific knockout mice were excised and first fixed in Bouin buffer for half an hour then in 10% formalin buffer. The fixed samples were processed to paraffin blocks, sectioned, and stained with hematoxylin-eosin (H&E).

The plasma triacylglycerol (TAG) level was measured using Serum Triglyceride Determination kit (Sigma) following the manufacturer's instructions. The NEFA level in serum was quantified by enzymatic assay kit (Wako). The serum insulin was determined using Rat/Mouse Insulin ELISA kit (Millipore) according to the instructions. Plasma glucose level was obtained using ACCU-CHEK Performa (Roche).

Measurement of metabolic parameters

Food intake, O_2 consumption, respiratory exchange rate (RER), energy expenditure and physical activity were determined using a TSE PhenoMaster/LabMaster system (Germany). Experiments were performed on control and AKO mice of 14-16 weeks in age. Mice were individually monitored for 72 hr and the data were collected in a time

interval of 27 min after one day adaption.

MRI and Computer tomography analysis

14-16 week-old male mice for the control (Ctrl) and adipose specific knockout of *Hdac6* (AKO) mice fed with a normal diet and high fat diets for 8 weeks were scanned using EchoMRI^{TM}-100H for the body composition measurement of fat and lean mass. *Lipin 1* knockout mice were scanned using Computer Tomography scan (Quantum FX microCT Imaging System, PerkinElmer) at 1 mm intervals x10 slices. The adipose tissues were three-dimensionally reconstructed and the quantities of subcutaneous fat, visceral fat, brown fat were calculated and total amount of adipose tissues were compared after normalization to mice body weight.

Glucose and insulin tolerance tests

GTT and ITT experiments were carried out in 14-16 weeks of Ctrl and AKO mice that were fed a normal chow diet. Animals were fasted for 16 hours and 4 hours for GTT and ITT experiments, respectively. Mice were then intraperitoneal injected with glucose (GTT, 1.0g per kg body weight) and recombinant human insulin (ITT, 0.5 units per kg body weight). Tail blood samples were collected at the indicated time points and blood glucose levels were measured according to manufacturer's instruction (ACCU-CHEK Performa (Roche).

Hyperinsulinemic euglycermic clamp

Hyperinsulinemic euglycemic clamps were performed as previously described (7, 8). Briefly, after implantation of dual catheters (MRE-025, Braintree Scientific) in the right jugular vein, the catheters were tunneled subcutaneously to the back of the neck and exteriorized. The mice were then allowed to recover for 5 days prior to clamp experiments. Following a 6 hour fast, the mice were infused with D-[3-^{3}H] glucose (Perkin Elmer Life Sciences, MA, USA) at a constant rate of 5 μCi/hr for 90 min. Blood was sampled at t=-10 and 0 min to determine basal glucose turnover. After the tracer equilibration, an infusion of glucose (50% glucose, variable infusion) and tracer

plus insulin were administrated at 5 μCi/hr and 8 mU/kg/min, respectively. Blood was collected from the tail vein every 10 min and analyzed for glucose. Blood collected at t=-10, 0 (basal), 110 and 120 (end of experiment) min was used to determine glucose-specific activity, insulin and free fatty acid (FFA) levels. The clamp was considered to have reached steady-state conditions (120 mg/dl ± 5 mg/dl) when glucose infusion and plasma glucose levels were maintained constant for at least 30 min. HGP and GDR were calculated in the basal state as well as steady-state. Tracer-determined rates were determined by using the Steele equation (9).

SVF (Stromal vascular fraction) isolation and differentiation

Stromal vascular fraction (SVF) contains adipocyte progenitors and was isolated as previous describe with slight modifications (10, 11). Briefly, gonadal white adipose tissue from four pairs of control or *Hdac6* adipose tissue specific knockout mice (AKO) were dissected, chopped into small pieces and mixed with digestion buffer for 30 minutes at 37℃. SVF cells were then collected by spinning the tissue digestion mixture for 5 minutes at 900 rpm. The collected cells were cultured in 24-well dish for two days or until they reached to confluence. Differentiation medium containing insulin, IBMX, dexamethasone and rosiglitazone was added into the cells to stimulate differentiation.

Production of AAV (Adeno-associated virus)

Adenovirus-associated viral (AAV) vector was obtained from Dr. X.W. Chen (Peking University, China). AAV-CMV-Flag-CIDEC, AAV-CMV-Flag-K56R plasmids were constructed by PCR the fragment from pCMV5-Flag-CIDEC and pCMV5-Flag-K56R. EcoR1 and BamH1 were used as the restriction sites for subcloning. The cloning primers were used as follows: forward 5'-CGGGATCCATGGACTACAAAGA-3' and reverse 5'-CGGAATTCTCATTGCAGCATCTT-3'. AAV was produced in HEK293T cells by the three plasmid based methods as previous described (12). Briefly, subconfluent cells were co-transfected with the three plasmids by using PEI. At 60h post-transfection, cells were collected and lysed by treating with benzonase. AAV was

purified via Iodixanol gradient centrifugation, at 50000 rpm for 1.5h at 16℃. Fractions of the virus were collected and diluted with 1×PBS, further concentrated in ultracentrifuge tube (Amacon 100k columns, UFC-910008). The purified and concentrated virus were aliquoted and stored at -80℃. Virus titers were determined by qPCR with primers corresponding to the insert sequences.

Mitochondrial isolation and measurement of oxygen consumption rate (OCR)

Isolation of the BAT mitochondria was performed according to previous description (13). Briefly, mitochondrial fraction was isolated in a mannitol-and sucrose-based MASE buffer and was assayed in MAS buffer. The mitochondrial oxygen consumption rate was measured using Seahorse XFe 96 (Agilent Technologies, USA) according to the manufacture's protocol (http://www.agilent.com/cs/library/technical-overviews/public/TB_Iso_Mito_XF96.pdf). Isolated mitochondria were added in the XFe 96 plate in an equal concentration of 3μg/well. Succinate/rotenone (10μM/2μM）was used as the substrate for respiration. The coupling assay was performed by injecting ADP (4mM), oligomycin (2.5μg/ml), FCCP (4μM), and antimycin A (4μM) sequentially.

Mitochondrial DNA (mtDNA) copy number

Mitochondrial DNA (mtDNA) copy number was evaluated by measuring the mtDNA level using real-time PCR analysis (14, 15). Method for the extraction of mitochondrial DNA and and specific primers for PCR analysis were described previously (16). The primer sequences for mtDNA were listed in the supporting table1. Gene *Apob* was used as a reference.

Fatty acid uptake and lipolysis

We carried out fatty acid uptake experiment according to the manufacture's protocol (Abcam, ab176768). Briefly, stromal vascular fraction (SVF) from the gonadal white adipose tissue were isolated and plated in a growth medium at $5*10^4$-$8*10^4$ cell/well/100 μL/96-well plate for 4-6 hours. Cells were differentiated into mature

adipocytes in vitro. Differentiated adipocytes were deprived of serum for one hour and fluorescent FA dye (Abcam, UK) was added into the culture medium for 1 hour and washed away. Fluorescence signal inside the cells was measured by a fluorescence microplate reader at Ex/Em=485/515nm (EnVision, PerkinElmer).

Lipolysis experiment was carried out on 12 week-old female mice as previously described (2). Blood samples from retro-orbital vein were collected from animals under fed condition, fasted for 8 hours or injected with isoproterenol at 5 μg per gram of body weight. Blood glycerol levels were measured using Free Glycerol Reagent (Sigma Aldrich, USA).

RNA extraction and Real-Time PCR

Total RNA was extracted from human tissue cells or mice tissues with TRIzol reagent (Invitrogen). The first-strand cDNA synthesis was performed with Superscript III RT kit and oligo-dT primers (Invitrogen). Real-Time PCR reaction was performed with the SYBR Green PCR system (Applied Biosystems) in an ABI 7500 thermal cycler (Applied Biosystems). β-actin was used as a reference gene. The primer sequences used are listed in Supporting Table 1.

siRNA experiments

Small interfering RNAs (siRNAs) were synthesized at GenePharma (China). We designed two different pairs of PCAF and HDAC6 which effectively knocked down genes at least 70% total protein. The sequences of siRNAs were listed in Supporting Table 2. The siRNAs were transfected into 3T3-L1 pre-adipocytes or differentiated adipocytes by on day 6 after induction of differentiation, electroporation for 48hr before processing other experiments.

Supporting Table1 Sequence of primers for Real-Time PCR

	Forward (5'-3')	Reverse (5'-3')
Actin	ACACTGTGCCCATCTACGAG	CAGCACTGTGTTGGCATAGAG
Cpt1	ACCACTGGCCGCATGT	CTCCATGGCGTAGTAGTTGCT
Cidea	TCCTCGGCTGTCTCAATG	TGGCTGCTCTTCTGTATCG
Ucp1	ACTGCCACACCTCCAGTCATT	CTTTGCCTCACTCAGGATTGG
Dio2	CAGTGTGGTGCACGTCTCCAATC	TGAACCAAAGTTGACCACCAG
Cpt2	CAGCACAGCATCGTACCCA	TCCCAATGCCGTTCTCAAAAT
Cidec	GTGTCCACTTGTGCCGTCTT	CTCGCTTGGTTGTCTTGATT
Cox4	CGGCGTGACTACCCCTTG	TGAGGGATGGGGCCATACA
Dgat1	TCCGTCCAGGGTGGTAGTG	TGAACAAAGAATCTTGCAGACGA
Dgat2	CTGGCTGATAGCTGCTCTCTACTTC	TGTGATCTCCTGCCACCTTTC
Hdac6	TCCACCGGCCAAGATTCTTC	CAGCACACTTCTTTCCACCAC
Hdac10	CCAGGGCATCCAGTATATCTTCA	CAACTCAGGATCAAACTCGAAGG
Cytc	CCAAATCTCCACGGTCTGTTC	ATCAGGGTATCCTCTCCCCAG
Acsl3	GGGACTACAATACCGGCAGA	ATAGCCACCTTCCTCCCAGT
Agpat4	ATGTCACCTGGTCTTCTGCTA	TTCGGGTCGGTGTAGATGGTA
Gpat4	AGCTTGATTGTCAACCTCCTG	CCGTTGGTGTAGGGCTTGT
Lipin1	CCCTCGATTTCAACGTACCC	GCAGCCTGTGGCAATTCA
Cd36	ATGGGCTGTGATCGGAACTG	GTCTTCCCAATAAGCATGTCTCC
Fas	GGAGGTGGTGATAGCCGGTAT	TGGGTAATCCATAGAGCCCAG
Acc1	GATGAACCATCTCCGTTGGC	GACCCAATTATGAATCGGGAGTG
Prdm16	CAGCACGGTGAAGCCATTC	GCGTGCATCCGCTTGTG
Tnfa	CCAGACCCTCACACTCAGATC	CACTTGGTGGTTTGCTACGAC
Cd11c	ACACAGTGTGCTCCAGTATGA	ACACAGTGTGCTCCAGTATGA
Mcp1	AGGTCCCTGTCATGCTTCTG	GCTGCTGGTGATCCTCTTGT
Il18	GACTCTTGCGTCAACTTCAAGG	CAGGCTGTCTTTTGTCAACGA
Il6	CCAGAGATACAAAGAAATGATGG	ACTCCAGAAGACCAGAGGAAAT

Il10	TGAATTCCCTGGGTGAGAAG	TCACTCTTCACCTGCTCCACT
Il4	ATGGAGCTGCAGAGACTCTT	AAAGCATGGTGGCTCAGTAC
Arg1	ATGGAAGAGACCTTCAGCTAC	GCTGTCTTCCCAAGAGTTGGG
Mrc2	TACAGCTCCACGCTATGGATT	CACTCTCCCAGTTGAGGTACT
Apob	CACGTGGGCTCCAGCATT	TCACCAGTCATTTCTGCCTTTG
mtDNA	CTCCGTGCTACCTAAACACCTTATC	GACCTAAGAAGATTGTGAAGTAGATGATG

Supporting Table 2 Sequence of siRNA for knock down experiments

	sense (5'-3')
si*Pcaf*(mouse)	GCAGAGGAGUCCUGUAAAU
si*Hdac6*(mouse)	CCGUGAAGGUGCCAACUUU
si*Pcaf*(human)	GCAUCCAAACAGUUAUCAA
si*Hdac6*(human)	GGUGUCACCUGAGGGUUAU
si*Cd36*	CCAGCCAAUGCCUUUGCAU
si*Dgat1*	GAUUCUUUGUUCAGCUCAGAC
si*Dgat2*	GACAUCUUCUCUGUCACCUGG
si*Fabp4*	GGGCUUUGCCACAAGGAAA

Supplemental References

1. Gong J, Sun Z, Wu L, Xu W, Schieber N, Xu D, Shui G, Yang H, Parton RG, and Li P. Fsp27 promotes lipid droplet growth by lipid exchange and transfer at lipid droplet contact sites. *J Cell Biol.* 2011;195(6):953-63.

2. Toh SY, Gong J, Du G, Li JZ, Yang S, Ye J, Yao H, Zhang Y, Xue B, Li Q, et al. Up-regulation of mitochondrial activity and acquirement of brown adipose tissue-like property in the white adipose tissue of fsp27 deficient mice. *PLoS One.* 2008;3(8):e2890.

3. Li JZ, Ye J, Xue B, Qi J, Zhang J, Zhou Z, Li Q, Wen Z, and Li P. Cideb regulates diet-induced obesity, liver steatosis, and insulin sensitivity by controlling lipogenesis and fatty acid oxidation. *Diabetes.* 2007;56(10):2523-32.

4. Nian Z, Sun Z, Yu L, Toh SY, Sang J, and Li P. Fat-specific protein 27 undergoes

ubiquitin-dependent degradation regulated by triacylglycerol synthesis and lipid droplet formation. *J Biol Chem.* 2010;285(13):9604-15.

5. Sun Z, Gong J, Wu H, Xu W, Wu L, Xu D, Gao J, Wu JW, Yang H, Yang M, et al. Perilipin1 promotes unilocular lipid droplet formation through the activation of Fsp27 in adipocytes. *Nature communications.* 2013;4(1594.

6. Kassan A, Herms A, Fernandez-Vidal A, Bosch M, Schieber NL, Reddy BJ, Fajardo A, Gelabert-Baldrich M, Tebar F, Enrich C, et al. Acyl-CoA synthetase 3 promotes lipid droplet biogenesis in ER microdomains. *J Cell Biol.* 2013;203(6):985-1001.

7. Li P, Lu M, Nguyen MT, Bae EJ, Chapman J, Feng D, Hawkins M, Pessin JE, Sears DD, Nguyen AK, et al. Functional heterogeneity of CD11c-positive adipose tissue macrophages in diet-induced obese mice. *J Biol Chem.* 2010;285(20):15333-45.

8. Li P, Oh da Y, Bandyopadhyay G, Lagakos WS, Talukdar S, Osborn O, Johnson A, Chung H, Mayoral R, Maris M, et al. LTB4 promotes insulin resistance in obese mice by acting on macrophages, hepatocytes and myocytes. *Nat Med.* 2015;21(3):239-47.

9. Steele R. Influences of glucose loading and of injected insulin on hepatic glucose output. *Ann N Y Acad Sci.* 1959;82(420-30.

10. Koh YJ, Koh BI, Kim H, Joo HJ, Jin HK, Jeon J, Choi C, Lee DH, Chung JH, Cho CH, et al. Stromal vascular fraction from adipose tissue forms profound vascular network through the dynamic reassembly of blood endothelial cells. *Arterioscler Thromb Vasc Biol.* 2011;31(5):1141-50.

11. Bunnell BA, Flaat M, Gagliardi C, Patel B, and Ripoll C. Adipose-derived stem cells: isolation, expansion and differentiation. *Methods.* 2008;45(2):115-20.

12. Huang X, Hartley AV, Yin Y, Herskowitz JH, Lah JJ, and Ressler KJ. AAV2 production with optimized N/P ratio and PEI-mediated transfection results in low toxicity and high titer for in vitro and in vivo applications. *J Virol Methods.* 2013;193(2):270-7.

13. Rogers GW, Brand MD, Petrosyan S, Ashok D, Elorza AA, Ferrick DA, and Murphy AN. High throughput microplate respiratory measurements using minimal quantities of isolated mitochondria. *PLoS One.* 2011;6(7):e21746.

14. Cree LM, Samuels DC, de Sousa Lopes SC, Rajasimha HK, Wonnapinij P, Mann JR, Dahl HH, and Chinnery PF. A reduction of mitochondrial DNA molecules during embryogenesis explains the rapid segregation of genotypes. *Nat Genet.* 2008;40(2):249-54.

15. He L, Chinnery PF, Durham SE, Blakely EL, Wardell TM, Borthwick GM, Taylor RW, and Turnbull DM. Detection and quantification of mitochondrial DNA deletions in individual cells by real-time PCR. *Nucleic Acids Res.* 2002;30(14):e68.

16. Machado TS, Macabelli CH, Sangalli JR, Rodrigues TB, Smith LC, Meirelles FV, and Chiaratti MR. Real-Time PCR Quantification of Heteroplasmy in a Mouse Model with Mitochondrial DNA of C57BL/6 and NZB/BINJ Strains. *PLoS One.* 2015;10(8):e0133650.

Data sheet S1

Summary of the acetylated-protein in *Hdac6* adipose tissue konckout mice related with lipid metabolism

Uniprot	Protein Names	Peptide sequence	Modifications	ΔCn	MH+ [Da]	Charge	Function Description
O88492	Perilipin-4 OS=Mus musculus GN=Plin4 PE=1 SV=2 - [PLIN4_MOUSE]	HMLIGMkDTVcAGVTSAMNmAkGIHk	K7(Acetyl); K22(Acetyl); K26(Acetyl)	2.73	2943.42	3	May play a role in triacylglycerol packaging into adipocytes. May function as a coat protein involved in the biogenesis of lipid droplets.
		SVLMGTKDTVTTGLTGAVNVAkGTIQGGLDTTk	K22(Acetyl); K33(Acetyl)	4.08	3318.77	5	
		SVVMGTkDTVTTGLTGAmNVAk	K7(Acetyl);K22(Acetyl)	2.58	2281.132	3	
P62204	Calmodulin OS=Mus musculus GN=Calm1 PE=1 SV=2 - [CALM_MOUSE]	HVMTNLGEkLTDEEVDEMIREADIDGDGQVNYEEFVQMMTAK	K9(Acetyl)	4.43	4872.229	5	Calmodulin mediates the control of a large number of enzymes, ion channels, aquaporins and other proteins by Ca2+. Among the enzymes to be stimulated by the calmodulin-Ca2+ complex are a number of protein kinases and phosphatases. Together with CCP110 and centrin, is involved in a genetic pathway that regulates the centrosome cycle and progression through cytokinesis
P09813	Apolipoprotein A-II OS=Mus musculus GN=Apoa2 PE=1 SV=2 - [APOA2_MOUSE]	QADGPDMQSLFTQYFQSMTDYGkDLmEkAK	K23(Acetyl); M26(Oxidation); K28(Acetyl)	2.55	3573.591	3	May stabilize HDL (high density lipoprotein) structure by its association with lipids, and affect the HDL metabolism.
Q9Z1B3-2	Isoform B of 1-phosphatidilinositol 4,5-bisphosphate phosphodiesterase beta-1 OS=Mus musculus GN=Plcb1 - [PLCB1_MOUSE]	VDSSNYMPQLFWNAGcQmVALNFQTVDLAmQINMGMYEYNGk	K42(Acetyl)	3.52	4953.262	5	The production of the second messenger molecules diacylglycerol (DAG) and inositol 1,4,5-trisphosphate (IP3) is mediated by activated phosphatidylinositol-specific phospholipase C enzymes.
Q61464-7	Isoform 6 of Zinc finger protein 638 OS=Mus musculus GN=Znf638 - [ZN638_MOUSE]	LASGTkPSAKSLSSVKSDSHLGAYSAHK	K6(Acetyl)	3.08	2856.443	4	Early regulator of adipogenesis that works as a transcription cofactor of CEBPs, controlling the expression of PPARG and probably of other proadipogenic genes, such as SREBF1. Binds to cytidine clusters in double-stranded DNA . May also regulate alternative splicing of target genes during adipogenesis
E9Q3L2	Protein Pi4ka OS=Mus musculus GN=Pi4ka PE=1 SV=1 - [E9Q3L2_MOUSE]	mmVQDLITALDHSHPQHYTQAMFk	K24(Acetyl)	2.84	2916.331	4	Acts on phosphatidylinositol (PtdIns) in the first committed step in the production of the second messenger inositol-1,4,5,-trisphosphate
Q8R3B1	1-phosphatidilinositol 4,5-bisphosphate phosphodiesterase delta-1 OS=Mus musculus GN=Plcd1 PE=2 SV=2 - [PLCD1_MOUSE]	LQEDckTIWQESR	K6(Acetyl)	2.17	1734.817	3	The production of the second messenger molecules diacylglycerol (DAG) and inositol 1,4,5-trisphosphate (IP3) is mediated by activated phosphatidylinositol-specific phospholipase C enzymes. Essential for trophoblast and placental development
A2AKK5	Acyl-coenzyme A amino acid N-acyltransferase 1 OS=Mus musculus GN=Acnat1 PE=1 SV=1 - [ACNT1_MOUSE]	GALFLPPGkGPFPGIIDLFGVIGGLVEFRASLLASHGFAVLALAYFAYK	K9(Acetyl)	3.74	5119.865	6	Acyltransferase which efficiently conjugates very long-chain and long-chain fatty acids to taurine. Shows no conjugation activity in the presence of glycine
F6V3Y9	Autophagy-related protein 2 homolog A (Fragment) OS=Mus musculus GN=Atg2a PE=1 SV=1 -	cTLDVIMPSAHIFLPSkEVYESIYNR	K17(Acetyl)	3.39	3124.601	3	Autophagy
E9QAK5	Kinesin-1 heavy chain (Fragment) OS=Mus musculus GN=Kif5b PE=2 SV=1 - [E9QAK5_MOUSE]	VSkTGAEGAVLDEAkNINK	K3(Acetyl); K15(Acetyl)	2.42	2028.031	3	Microtubule-dependent motor required for slow axonal transport of neurofilament proteins
F7A3M3	Apolipoprotein B-100 (Fragment) OS=Mus musculus GN=Apob PE=4	LDLAGSLDGQLWDLEAIFLPVYGk	K24(Acetyl)	2.41	2675.383	3	
P27656	Hepatic triacylglycerol lipase OS=Mus musculus GN=Lipc PE=2 SV=2 - [LIPC_MOUSE]	IPITLGEGITSNKTYSFLITLDKDIGELILLk	K32(Acetyl)	2.88	3561.065	6	Hepatic lipase has the capacity to catalyze hydrolysis of phospholipids, mono-, di-, and triglycerides, and acyl-CoA thioesters. It is an important enzyme in HDL metabolism. Hepatic lipase binds heparin.
Q8K449	ATP-binding cassette sub-family A member 9 OS=Mus musculus GN=Abca9 PE=2 SV=2 -	GLGFDIYEGQITALLGHSGAGk	K22(Acetyl)	2.39	2246.135	3	May play a role in monocyte differentiation and lipid homeostasis
Q8CHP8	Glycerol-3-phosphate phosphatase hydrolyzing glycerol-3-phosphate into glycerol. Thereby, regulates the cellular levels of glycerol-3-phosphate a metabolic intermediate of glucose, lipid and energy metabolism . Was also shown to have a 2-phosphoglycolate	LSAERAk	K7(Acetyl)	2.07	816.4576	2	Phosphoglycolate phosphatase OS=Mus musculus GN=Pgp PE=1 SV=1 - [PGP_MOUSE]
Q3U1N2-2	Isoform 2 of Sterol regulatory element-binding protein 2 OS=Mus musculus GN=Srebf2 - [SRBP2_MOUSE]	TDGSPVMAAVQNPALTALTAPIQTAALQVPTLVGSNGTILTTMPVMmGQEkVPIk	K51(Acetyl); K55(Acetyl)	2.84	5672.892	5	Transcriptional activator required for lipid homeostasis. Regulates transcription of the LDL receptor gene as well as the cholesterol and to a lesser degree the fatty acid synthesis pathway. Binds the sterol regulatory element 1 (SRE-1) (5'-ATCACCCCAC-3') found in the flanking region of the LDRL and HMG-CoA synthase genes
Q3TFD2	Lysophosphatidylcholine acyltransferase 1 OS=Mus musculus GN=Lpcat1 PE=1 SV=1 - [PCAT1_MOUSE]	AQVAFmTLTLFPIRLLFAAFmMLLAWPFALLASLGPPDkEPEQPLALWR	K39(Acetyl)	4.63	5615.898	7	Possesses both acyltransferase and acetyltransferase activities. Activity is calcium-independent. Mediates the conversion of 1-acyl-sn-glycero-3-phosphocholine (LPC) into phosphatidylcholine (PC) . Displays a clear preference for saturated fatty acyl-CoAs, and 1-myristoyl or 1-palmitoyl LPC as acyl donors and acceptors, respectively. May synthesize phosphatidylcholine in pulmonary surfactant, thereby playing a pivotal role in respiratory physiology . Involved in the regulation of lipid droplet number and size
Q9D061-2	Isoform 2 of Acyl-CoA-binding domain-containing protein 6 OS=Mus musculus GN=Acbd6 - [ACBD6_MOUSE]	VGNcNTPkPNFFDFEGK	K8(Acetyl)	2.5	2012.892	3	Binds long-chain acyl-coenzyme A molecules with a strong preference for unsaturated C18:1-CoA, lower affinity for unsaturated C20:4-CoA, and very weak affinity for saturated C16:0-CoA. Does not bind fatty acids
Q6RI63-2	Isoform 2 of Constitutive coactivator of peroxisome proliferator-activated receptor gamma OS=Mus musculus GN=Fam120b - [F120B_MOUSE]	GVTSYLLPGQkSPWLVQkPkGMITDK	K11(Acetyl); K18(Acetyl); K20(Acetyl)	2.67	2997.632	5	unctions as a transactivator of PPARG and ESR1. Functions in adipogenesis through PPARG activation
P56198	Cell death activator CIDE-3 OS=Mus musculus GN=Cidec PE=1 SV=2 - [CIDEC_MOUSE]	KGIMAHSLEDLLNK	K1(Acetyl)	3.18	1568.844	3	Binds to lipid droplets and regulates their enlargement, thereby restricting lipolysis and favoring storage. At focal contact sites between lipid droplets, promotes directional net neutral lipid transfer from the smaller to larger lipid droplets. The transfer direction may be driven by the internal pressure difference between the contacting lipid droplet pair. Its role in neutral lipid transfer and lipid droplet enlargement is activated by the interaction with PLIN1.
		AQLALSQKPTkK	K11(Acetyl)	4.23	1354.803	2	